Optimizing the operation of a spark ignition engine: Simulation and theoretical tools

P. L. Curto-Risso,[a)] A. Medina,[b)] and A. Calvo Hernández[c)]
Departamento de Física Aplicada, Universidad de Salamanca, 37008 Salamanca, Spain

By performing quasidimensional computer simulations and finite-time thermodynamic analysis we study the effect of spark advance, fuel ratio, and cylinder internal wall temperature in spark ignition engines. We analyze the effect of these parameters on the power output and efficiency of the engine at any rotational speed, ω. Moreover, we propose the optimal dependence on ω of the spark advance angle and the fuel ratio with the objective to get maximum efficiency for any fixed power requirement. The importance of engine power-efficiency curves in order to perform this optimization procedure and also of the evaluation of macroscopic work losses in order to understand the physical basis of the optimization process is stressed. Taking as reference results from simulations with constant standard values of spark advance, fuel ratio, and cylinder internal wall temperature, the optimized parameters yield to substantial increases in engine performance parameters. © *2009 American Institute of Physics*. [DOI: 10.1063/1.3116560]

I. INTRODUCTION

From its historical origin Otto's four-stroke engine (and in general spark ignition engines) have evolved very successfully. In the early times, designers were especially involved with the increase in engine power and obtaining a good working reliability. These objectives have changed in the past three decades because of the new strict emission standards and the fuel shortage problem. Optimization of the engine design and operation variables needs extensive engine testing. Computer simulations of the physical processes involved in engine operation are interesting tools for the analysis and optimization of engine performance[1] since they allow to check and develop the design of the engine and its operation alternatives in an inexpensive way. Furthermore, numerical models give us a better understanding of the complex physical mechanisms involved in the operation of a real engine.

Also theoretical methods such as thermodynamic optimization or finite-time thermodynamics (FTT)[2–4] constitute an interesting approach because, from the consideration of simple models, they provide useful insights about the performance and optimization of real heat devices. One of the goals of FTT is to determine more realistic bounds for thermodynamic performance than those obtained from traditional thermodynamics of equilibrium. This is done by focusing attention on the irreversibilities affecting heat engines and proceeding in a finite time or with finite rates. It is desirable to develop this procedure keeping models simple but sufficiently close to realistic results to provide useful insights. Another point to pay attention is the finding of opti-

mal values for the main variables of engine operation or design. In FTT it is usual to propose optimization criteria, defining an objective function with a clear physical meaning such as thermal efficiency, power, power density, ecological functions, thermoeconomical functions, etc.,[5] depending on the variables of the system and thus susceptible to be optimized. Recently, it was shown that FTT techniques, with the inclusion of a reduced set of macroscopic parameters depending on the rotational speed of the engine, are capable to reproduce the results of a quasidimensional simulation of a spark ignition engine that includes explicitly combustion.[6,7]

From a global perspective, the objective of this paper is to simultaneously make use of the capabilities of two different techniques to model real spark engines. On one hand, numerical simulations based on the resolution of a set of differential coupled differential equations for the temperature and pressure inside the cylinder at any time and, inclusively, at any position,[1,8–10] and on the other hand, FTT macroscopic approach from the basis of classical thermodynamics and performance records are obtained from first principles assuming simple models for the irreversibilities affecting engine evolution.

Recently, Descieux and Feidt[11] performed a *one-zone* simulation of a compression ignition engine and analyzed the evolution of the corresponding power-efficiency curves with several parameters, some of them related to engine design and other related to engine operation. In this work we shall make use of a quasidimensional *two-zone* computer simulation, previously developed and validated,[6] that includes turbulent combustion, in order to analyze the influence of three basic parameters on the power output and efficiency of the engine: spark advance, fuel ratio, and cylinder internal wall temperature. Then, from the results of simulations, we apply usual FTT techniques with the aim to propose optimal values for the checked variables. Those techniques include the macroscopic definition and analysis of work losses associated with the main irreversibility sources and the analysis of

---
a)Also at Instituto de Ingeniería Mecánica y Producción Industrial, Universidad de la República Oriental del Uruguay. Electronic mail: pcurto@fing.edu.uy.
b)Also at ETSII de Béjar, Universidad de Salamanca, 37700 Béjar, Salamanca, Spain. Electronic mail: amd385@usal.es.
c)Electronic mail: anca@usal.es.

power-efficiency implicit curves.[11,12] We shall numerically calculate the improvement on power output and engine efficiency when we compare results obtained with standard constant (speed independent) parameters and those optimal speed dependent parameters obtained by means of FTT theoretical tools. The importance of the analysis of power-efficiency curves in this optimization procedure because they support a clear way to obtain the maximum achievable efficiency for a certain fixed power requirement, provided that in a real engine power requirements depend on the operating conditions, will be stressed. The merged use of both approaches shall allow us, apart to propose concrete values for optimal parameters (always interesting from the viewpoint, for instance, of system control),[13] to physically understand the basis of the optimization procedure and its consequences.

The paper is organized in the following way. Section II is devoted to briefly describe the basic elements of our quasidimensional computer simulation. In Sec. III we explain how to evaluate macroscopic work losses during engine operation from the simulations. Section IV contains the main numerical results of the paper, relative to the influence on engine performance of the spark advance, the fuel ratio of the mixture, and the cylinder internal wall temperature. Finally, in Sec. V, we deepen in the results of the optimization procedure and summarize the main conclusions of the paper.

II. COMPUTER SIMULATION OF A SPARK IGNITION ENGINE

We model a spark ignition piston-cylinder system performing a four-stroke cycle. Considering a two-zone model for combustion,[10] i.e., distinguishing between unburned (u) or burned (b) gases, we apply the first principle of thermodynamics for open systems taking the cylinder interior as a control volume. The working fluid is considered as an adiabatic mixture (except during combustion period) of ideal gases, unburned and burned. The gas constant of each chemical species is considered as temperature and pressure independent (and so the gas constant of the unburned gas mixture, R_u), although the gas constant of the burned gases R_b does depend on the chemical composition of exhaust gases, which in turn is a function of temperature. The fuel ratio ϕ is also taken as a constant and enthalpy changes are only associated with temperature variations except during combustion.

Considering that initial pressure and temperature are fixed by external conditions, coupled differential equations for the control volume are the following:

$$\frac{dT}{dt} = \frac{1}{(m_u c_{p,u} + m_b c_{p,b})} \left[\dot{Q}_u + \dot{Q}_b + \dot{m}_{in}h_{in} + \dot{m}_{ex}h_{ex} \right.$$
$$\left. - \dot{m}_u h_u - \dot{m}_b h_b + V\frac{dp}{dt} \right], \quad (1)$$

$$\frac{dp}{dt} = \left[p\left(\frac{\dot{m}_u}{\rho_u} + \frac{\dot{m}_b}{\rho_b} - \frac{dV}{dt}\right) + (\dot{Q}_u + \dot{Q}_b + \dot{m}_{in}h_{in} + \dot{m}_{ex}h_{ex} \right.$$
$$\left. - \dot{m}_u h_u - \dot{m}_b h_b) \right]\left[V\left(1 - \frac{V}{\frac{V_u c_{p,u}}{R_u} + \frac{V_b c_{p,b}}{R_b}}\right)\right]^{-1}, \quad (2)$$

where c_p denotes specific heat capacity, h denotes specific enthalpy, ρ denotes gas density, and V denotes cylinder volume. These equations are applicable to any period of system evolution unless combustion, which will be considered further. Moreover, they are valid either for unburned or burned gases, even during the overlapping period where intake and exhaust valves are simultaneously open. Terms depending on $\dot{m}_u$ or $\dot{m}_b$ are associated with enthalpy changes inside the cylinder and terms with $\dot{m}_{in}$ or $\dot{m}_{ex}$ arise from intake or exhaust processes. Depending on the relative pressures between cylinder interior and external conditions $\dot{m}_{in}$ and $\dot{m}_{ex}$ can be positive or negative. Terms $\dot{Q}_u$ and $\dot{Q}_b$ emerge from heat losses of unburned or burned gases. Each term in the equations labeled with u or b can be zero or not in any particular stroke. For instance, when unburned gases are not present inside the cylinder, $m_u=0$ and $\dot{Q}_u=0$. The same is true for burned gases.

During combustion two control volumes, separated by the flame front, are considered.[14] So, different temperature equations for unburned or burned gases are formulated. Apart from sensible enthalpy changes, now chemical variations of enthalpy are also taken into account,

$$\frac{dT_u}{dt} = \frac{\dot{Q}_u + V_u \dfrac{dp}{dt}}{m_u c_{p,u}}, \quad (3)$$

$$\frac{dT_b}{dt} = \frac{\dot{Q}_b + \dot{m}_b(h_u - h_b) + V_b \dfrac{dp}{dt}}{m_b c_{p,b}}, \quad (4)$$

$$\frac{dp}{dt} = \left[p\left(\frac{\dot{m}_b}{\rho_b} + \frac{\dot{m}_u}{\rho_u} - \frac{dV}{dt}\right) + \frac{\dot{Q}_u R_u}{c_{p,u}} \right.$$
$$\left. + (\dot{Q}_b + \dot{m}_b(h_u - h_b))\frac{R_b}{c_{p,b}} \right]\left(V - \frac{V_u R_u}{c_{p,u}} - \frac{V_b R_b}{c_{p,b}}\right)^{-1}. \quad (5)$$

The initial value of T_b is taken as the adiabatic flame temperature at constant pressure.[15]

The resolution of all these thermodynamic equations requires the consideration of particular models for any of the four strokes of the piston evolution (see Ref. 6 for details). We only observe here that we deal with the stationary evolution of the engine at a fixed rotational speed, so a differential equation for the mechanics of the system is not necessary. From the mechanical point of view the only relation to be specified is that between the volume inside the cylinder, V, and the crankshaft angle, φ.[6] Also, mass flow rates are calculated through a one-dimensional isentropic flow analysis, from the standard equations for a compressible flow

through a restriction.[1] Next we detail the main assumptions considered in the model of the combustion process, heat transfers, and engine friction.

A. Combustion model

For simulating combustion we assume the quasidimensional model proposed by Keck and co-worker[16,17] and developed by Beretta et al.,[18] sometimes called *eddy-burning* model. The combustion is considered as turbulent. During flame propagation not all the mass inside the approximately spherical flame front is burned, but there exist unburned eddies of typical length l_t. Thus, a set of coupled differential equations for the time evolution of total mass within the flame front, m_e (unburned eddies plus burned gas), and burned mass, m_b, is solved as follows:

$$\dot{m}_b = A_f \rho_u S_l + \frac{m_e - m_b}{\tau_b}, \tag{6}$$

$$\dot{m}_e = A_f \rho_u (u_t + S_l), \tag{7}$$

where A_f is the area of the spherical flame front, which is calculated from its radius, and this in turn from the volume of the gases inside the flame front,[14] $V_f = V_b + (m_e - m_b)/\rho_u$ where $V_b = m_b/\rho_b$ is the volume of the burned gas mixture. The first term in Eq. (6) stands for the laminar propagation forward of the approximately spherical flame front, and the second term represents the burning of the mixture already entrained within this flame front. τ_b is a characteristic time for the combustion of a typical length eddy l_t at a velocity S_l. Also τ_b represents the time required for the flame front to develop into a turbulent flame from the initial laminar and spherical conditions.[19] Equation (7) describes the rate of change in the total gas mixture within the flame front at a velocity $u_t + S_l$, where u_t is the characteristic (convective) velocity at which fresh mixture crosses the flame front and S_l is the laminar (diffusive) flame speed. Of course, during combustion, these equations are also coupled with the thermodynamic ones.

B. Heat transfer model

Another model to specify in order to solve the set of thermodynamic differential equations is the heat transfer between the gas mixture inside the cylinder and the walls. Among the several models that can be found in literature for four-stroke spark ignition engines, we shall consider that due to Eichelberg,[20] because it only requires to fix a mean inner surface temperature T_w,

$$\frac{\dot{Q}_s}{A_s} = 2.43 v_p^{1/3} (pT)^{1/2} (T - T_w), \tag{8}$$

where $\dot{Q}_s$ represents the instantaneous heat flow rate, A_s is the instantaneous surface transfer area, p is the instantaneous pressure inside the cylinder in bar, and T is the instantaneous bulk gas temperature. $v_p = (2/\pi)\omega a$ is the mean piston speed, a is the crankshaft radius, and ω is the angular velocity. The units of all variables except pressure are international system units.

C. Friction model

We assume that friction forces exerted on the piston linearly depend on its instantaneous speed, i.e., we do not consider neither constant (boundary friction) nor speed squared terms (pumping turbulent dissipations) as Descieux and Feidt[11] recently did for a Diesel engine. So, $|F_{\text{fric}}| = \mu |\dot{x}|$ where μ is an effective friction coefficient (that we shall consider temperature independent as most authors do[1,11]), and $x(t)$ is the position of the piston with respect to the bottom center at time t.[6] The effect of friction forces on the net work is

$$|W| = |W_{\text{gas}}| - |W_{\text{fric}}|, \tag{9}$$

where, in terms of the crankshaft angle φ and piston section A_p,

$$|W_{\text{gas}}| = \left| \int_0^{4\pi} p \left(\frac{dV}{d\varphi} \right) d\varphi \right|, \tag{10}$$

$$|W_{\text{fric}}| = \frac{1}{A_p} \int_0^{4\pi} |F_{\text{fric}}| \left| \frac{dV}{d\varphi} \right| d\varphi. \tag{11}$$

III. ANALYSIS OF LOSSES

Following, the usual procedures of finite-time thermodynamics,[6,11,21,22] we shall quantify work losses associated with thermodynamic irreversibilities during engine evolution by taking the reversible Otto cycle as a reference. This cycle is performed by certain mass of an ideal gas undergoing two isochoric processes, combustion $(2 \rightarrow 3)$ and cooling $(4 \rightarrow 1)$, and two adiabatic branches corresponding to compression $(1 \rightarrow 2)$ and power stroke $(3 \rightarrow 4)$. Intake and exhaust processes do not affect calculations of power or efficiency because they are supposedly isobaric and the pressure difference is small.

The shape and size of the cycle can be characterized by two geometrical parameters, a compression ratio, $r = V_1/V_2 = V_4/V_3 \geq 1$, and, the ratio between cycle extreme temperatures, $\tau = T_1/T_3 \leq 1$. To compare the simulated cycle with the PV-diagram of the theoretical Otto cycle, we fix r as an input parameter of the simulation, and temperatures are obtained in the following manner (see Refs. 6 and 23). Temperature T_1 is calculated from the simulation as the temperature of the gases within the cylinder when piston reaches the bottom center. The temperature at the beginning of the combustion stroke, T_2, is obtained from T_1 and the adiabatic equation $T_2 = T_1 r^{\bar{\gamma}_{12}-1}$ and maximum temperature of the cycle, and T_3 is estimated by numerically solving $0 = U_P(T_3) - U_R(T_2)$, where $U_P(T)$ and $U_R(T)$ are, respectively, the tabulated internal energies (including the chemical term) of products and reactants at those temperatures. This implies that all internal energy from reactants, chemical and sensible, is transferred to products. With these considerations, the computed *reversible* work is calculated as for a standard Otto cycle,[6]

$$|W_{\text{rev}}| = T_3 [\bar{C}_{v,23}(1 - \tau r^{\bar{\gamma}_{u,12}-1}) - \bar{C}_{v,41}(r^{1-\bar{\gamma}_{b,34}} - \tau)], \tag{12}$$

where heat capacities and adiabatic coefficients are calculated as temperature averages over the considered tempera-

ture interval and for the corresponding chemical species, considering the composition of the mixture in the cylinder before (u) and after (b) combustion. For instance,[23]

$$\bar{C}_{v,23} = \frac{1}{2}[C_{v,u}(T_2) + C_{v,b}(T_3)],$$

$$\bar{\gamma}_{12} = \frac{\bar{C}_{p,12}}{\bar{C}_{v,12}} = \frac{C_{p,u}(T_1) + C_{p,u}(T_2)}{C_{v,u}(T_1) + C_{v,u}(T_2)}. \tag{13}$$

We have checked that this simplification does not modify the results of simulations with respect to the parameters we are interested in (power, efficiency, and work losses).

As in previous FTT works[6,21] we assume three main irreversibility sources: frictions between piston and cylinder walls, heat transfers from the working fluid to the surroundings, and working fluid internal irreversibilities. These internal losses[22,23] include all other losses related to the working fluid but not associated with its coupling with the external reservoirs, for instance, those arising from considering the combustion as turbulent or from the nonideal flows through engine valves. Next we detail how to evaluate either internal or external irreversibilities from our simulation model.

The lost work associated with friction between the piston and the cylinder walls can be directly calculated from simulations through Eq. (11). To quantify work losses from internal irreversibilities we calculate from simulations the net work $|W_I|$ obtained from the cycle when neither piston-cylinder frictions nor heat transfers are computed. Then, the difference $|W_{int}| = |W_{rev}| - |W_I|$ quantifies all other work losses that we consider as coming from fluid internal irreversibilities. Finally, to calculate the lost work arising from the heat transfers from the working fluid to the surroundings, we define

$$|W_Q| = |W_I| - |W_{fric}| - |W|, \tag{14}$$

where $|W|$ is the net work obtained from the simulation when all effects are considered simultaneously: internal, friction, and heat transfer. We can also define a net lost work $|W_\ell|$ as

$$|W_\ell| = |W_{int}| + |W_{fric}| + |W_Q|. \tag{15}$$

The efficiency of the engine is obtained from

$$\eta = \frac{|W|}{m_{fuel}|Q_{LHV}|}, \tag{16}$$
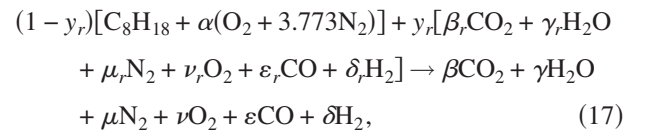
where $|Q_{LHV}|$ is the lower isochoric calorific value of the fuel.[24] As we shall see in Secs. IV and V we are interested in the operation of the engine at any fixed angular velocity ω. So, in order to evaluate the particular engine efficiency at a given ω, we take an average value by repeating the simulation several times, calculating for each one the net work $|W|$ and the mass of fuel inside the cylinder after closing the intake valve, m_{fuel}. $|Q_{LHV}|$ is the same in each cycle because it only depends on the type of fuel considered. Note that this measure of engine efficiency actually represents a *fuel conversion efficiency* because the denominator of Eq. (16) is the fuel energy, which can be released by the combustion of the fuel mass in the engine per cycle.[25,26]

TABLE I. Geometrical and configuration parameters of the simulations.

V_{cyl}, cylinder volume	8.0×10^{-4} m^3
a, crank radius	4.8×10^{-2} m
B, piston bore	9.6×10^{-2} m
r, compression ratio	8
μ, friction coefficient	16.0 kg/s
p_{in}, intake pressure	0.75×10^5 Pa
T_{in}, intake temperature	350.0 K
p_{ex}, exhaust pressure	1.05×10^5 Pa
T_{ex}, exhaust temperature	600 K

IV. NUMERICAL RESULTS

To run the simulations we elect the reference fuel for Otto based engines, iso-octane, C_8H_{18}, considering the unburned gas mixture composed by fuel, air, and residual gases

$$(1 - y_r)[C_8H_{18} + \alpha(O_2 + 3.773N_2)] + y_r[\beta_r CO_2 + \gamma_r H_2O$$
$$+ \mu_r N_2 + \nu_r O_2 + \varepsilon_r CO + \delta_r H_2] \rightarrow \beta CO_2 + \gamma H_2O$$
$$+ \mu N_2 + \nu O_2 + \varepsilon CO + \delta H_2, \tag{17}$$

where the subscript r refers to *residual* and y_r is the molar fraction of exhaust gases in the intake process. The program CEA developed by NASA (Ref. 27) was employed to solve combustion and to calculate exhaust composition.

The thermodynamic properties of all chemical species, considered as ideal gases, are obtained from the constant pressure specific heat, which is expressed always as a seven parameter temperature polynomial.[27] The thermodynamic set of coupled differential equations is solved by means of a fourth-order Runge–Kutta algorithm. Table I contains the main geometrical and configuration parameters required to run simulations. All other parameters can be found in Ref. 6, as well as details about the validation of the simulation.

In Secs. IV A–IV C we present the main results on the influence of spark advance, the fuel-air equivalence ratio and the internal cylinder wall temperature on the power output and efficiency of the engine, and also the analysis of how to optimize these performance parameters in order to get the maximum achievable efficiency for each required power output.

A. Spark advance

The location of the combustion event relative to the top center (TC) (that is often taken as 360°) is a basic parameter in order to obtain maximum achievable power or torque. Usually combustion starts before the end of the compression stroke, and its duration is between 30 and 90 crank angle degrees, finishing after the maximum pressure point in the cycle. If combustion is progressively advanced before the TC, the work from the piston to cylinder gases during the compression stroke increases. On the contrary, if spark timing is retarded, pressure peak appears later in the expansion stroke and moreover its maximum value decreases. As a consequence, useful work during the power stroke is reduced. Normally, spark advance angle is in the range between intake valve closure (around 220°) and TC.
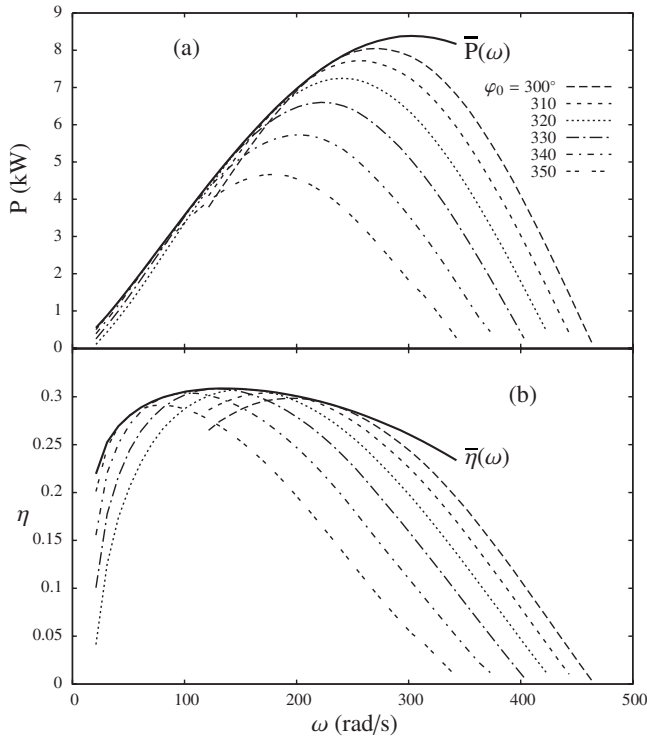
FIG. 1. (a) Power output of the simulated engine as a function of engine rotational speed, ω, for different spark advance angles, φ_0, as shown in the inset (in degrees). The envelope $\bar{P}=\bar{P}(\omega)$, obtained with the optimized speed dependent ignition delay $\bar{\varphi}_0(\omega)$, is also shown (see text for details on the optimization procedure). (b) Corresponding results for engine efficiency. All curves were obtained with constant values of fuel ratio $\phi=1.0$ and cylinder internal wall temperature $T_w=500$ K.

Most usual analysis of the optimal timing are made at a fixed engine speed, as for instance, that giving maximum brake torque (MBT timing[28]) that takes place when the above mentioned effects offset each other. Our aim here is to consider with some extent the influence on the optimization process of both the rotational speed ω and the spark advance angle φ_0. From our simulations we can obtain the behavior of $P(\omega,\varphi_0)$ and $\eta(\omega,\varphi_0)$ at any given value of φ_0. A set of curves for those functions at several particular values of φ_0 is plotted in Fig. 1(a) for power and Fig. 1(b) for efficiency. From each of these curves it would be easy to obtain the optimum value of ω giving maximum power or efficiency for a particular φ_0. Proceeding in this way (that would be the usual one in the framework of FTT), ω behaves as an independent variable of the problem and φ_0 would be a parameter of control.

However, the versatility of simulations allows for a step further in the optimization of power or efficiency by considering a suitable, explicit dependence of φ_0 on ω. We can look for functions $\bar{\varphi}_0^P(\omega)$ or $\bar{\varphi}_0^\eta(\omega)$ so that $P[\omega,\bar{\varphi}_0^P(\omega)]$ or $\eta[\omega,\bar{\varphi}_0^\eta(\omega)]$ reach the maximum achievable values for any rotational speed. It is easy to understand this procedure by thinking in geometrical terms. We shall try to get the functions $\bar{\varphi}_0^P(\omega)$ or $\bar{\varphi}_0^\eta(\omega)$ that lead to the envelopes of the set of curves of Fig. 1(a) or Fig. 1(b). We denote these envelopes by $\bar{P}(\omega)$ and $\bar{\eta}(\omega)$. They verify that for any value of ω are the maximum reachable values of power output or efficiency and can be obtained in the following way: In the set of
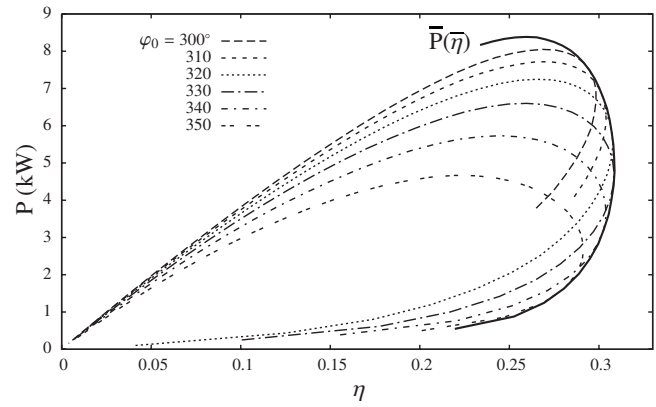

FIG. 2. Power-efficiency curves $P=P(\eta)$, obtained by eliminating ω between $P=P(\omega)$ and $\eta=\eta(\omega)$ for the same spark advanced angles as those in Fig. 1. The envelope $\bar{P}=\bar{P}(\bar{\eta})$ is obtained by taking the optimal speed dependent spark advance $\bar{\varphi}_0(\omega)$.

curves for power or efficiency obtained with the fixed values of φ_0 we can take for each ω the value of φ_0 giving maximum power or efficiency, thus building a discrete number of pairs $(\omega,\bar{\varphi}_0^P)$ or $(\omega,\bar{\varphi}_0^\eta)$. Afterwards, it is straightforward to perform a numerical interpolation to obtain the functions $\bar{\varphi}_0^P(\omega)$ or $\bar{\varphi}_0^\eta(\omega)$. When running the simulations with these ω-dependent values of the spark advance we get the envelopes shown in Figs. 1(a) and 1(b), $\bar{P}[\omega,\bar{\varphi}_0^P(\omega)]$ or $\bar{\eta}[\omega,\bar{\varphi}_0^P(\omega)]$.

It is worth mentioning that both functions, $\bar{\varphi}_0^P(\omega)$ and $\bar{\varphi}_0^\eta(\omega)$, result to be numerically very similar, almost indistinguishable and with a quite simple, linear form, $\bar{\varphi}_0^P(\omega) \simeq \bar{\varphi}_0^\eta(\omega)=363.85-0.27\omega$, with φ_0 in deg and ω in rad/s. Note that in the limit $\omega\to0$, the thermodynamic cycle developed by the engine corresponds to the Otto reversible cycle (performed in an infinite time), and in this case $\bar{\varphi}_0^P$ should be $360°$, i.e., combustion begins when piston is at the TC. In our case this limit yields to a slightly different value due to the biparametric linear fitting procedure.

Because of the numerical similitude between those optimal spark advance functions, $\bar{\varphi}_0^P(\omega)\simeq\bar{\varphi}_0^\eta(\omega)\equiv\bar{\varphi}_0(\omega)$, it is possible to consider this function as an optimal spark advance function giving maximum possible power and maximum possible efficiency simultaneously at each given rotational speed. The joint optimization of power and efficiency does not offer any inconsistency, since as shown in Eq. (16), $\eta=|W|/(m_{fuel}|Q_{LHV}|)$, efficiency is related to work (or power) through the mass of fuel inside the cylinder that is independent of spark advance. So, in regard to the spark advance angle, optimization of engine efficiency or power output should lead to the same result, as it is confirmed by the results mentioned above. In Sec. IV B we shall see that this is not true for the fuel-air equivalence ratio ϕ, since m_{fuel} does depend on ϕ.

In Fig. 2 we plot parametric power-efficiency curves $P(\eta,\varphi_0)$ obtained by eliminating ω between $P(\omega,\varphi_0)$ and $\eta(\omega,\varphi_0)$ for the considered values of spark advance. The envelope of these curves, $\bar{P}=\bar{P}(\bar{\eta})$, is also shown. It is obtained by taking the optimal spark advance for each engine speed, i.e., eliminating ω between $\bar{P}(\omega)$ and $\bar{\eta}(\omega)$ or equiva-
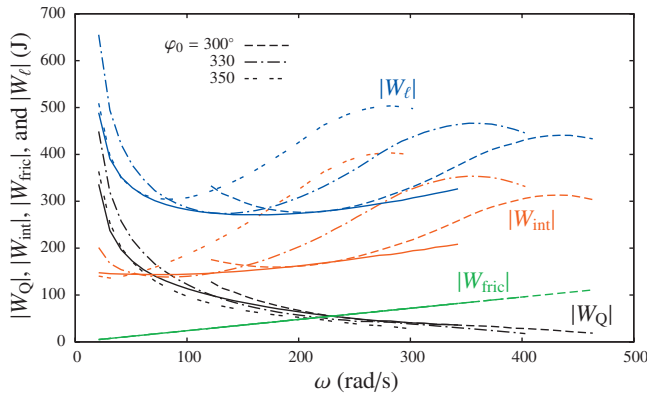
FIG. 3. (Color) Analysis of work losses as function of engine speed for some spark advance angles as defined in Sec. III. For each type of losses, those obtained with the optimized spark advance angle $\bar{\varphi}_0(\omega)$ are shown in solid line. All curves were obtained with constant values of fuel ratio ϕ =1.0 and cylinder internal wall temperature T_w=500 K.

lently by running the simulation with the optimal variable spark advance $\bar{\varphi}_0(\omega)$. For a given value of power output (i.e., considering it as an externally fixed parameter) this envelope always give us the maximum reachable engine efficiency. For the sake of consistency, all the results we present in Secs. IV B and IV C were obtained with this optimal speed dependent spark advance.

It is very interesting to analyze the optimization procedure in terms of work losses as theoretically introduced in Sec. III. As an illustration we depict in Fig. 3 work losses associated with heat transfer $|W_Q|$, frictions $|W_{\text{fric}}|$, and internal irreversibilities $|W_{\text{int}}|$, as well as the addition of all work losses $|W_\ell|$ [see Eq. (15)], for three values of φ_0 and for $\bar{\varphi}_0(\omega)$. From this figure important conclusions can be obtained.

(i)   At low rotational speeds total losses (dashed blue lines) are dominated by heat transfer (dashed black lines), but at intermediate and high speeds, the internal irreversibilities (dashed red lines) become the most important contribution to total losses. Friction losses (dashed green lines) are independent of φ_0 and monotonically increase with ω.

(ii)   When the engine runs with the optimal spark timing, $\bar{\varphi}_0(\omega)$ (solid lines), heat or internal losses are practically minimized: at low ω those coming from heat losses and at intermediate and high ω those arising from internal irreversibilities. As a straightforward consequence the addition of all losses $|W_\ell|$ retains the minimum possible value at any rotational speed.

(iii)   The observed envelope in $|W_\ell|$ generated by the consideration of the optimal $\bar{\varphi}_0(\omega)$ for the different spark advance angles can be understood as the complementary version of the one showed by $\bar{P}(\bar{\eta})$ (Fig. 2) in terms of minimum work losses instead of maximum power and efficiency. Thus, the optimization procedure physically could be understood as a mechanism to minimize total losses by reducing heat transfer or internal irreversibility losses as functions of the engine rotational speed in the different operation regimes of the engine.
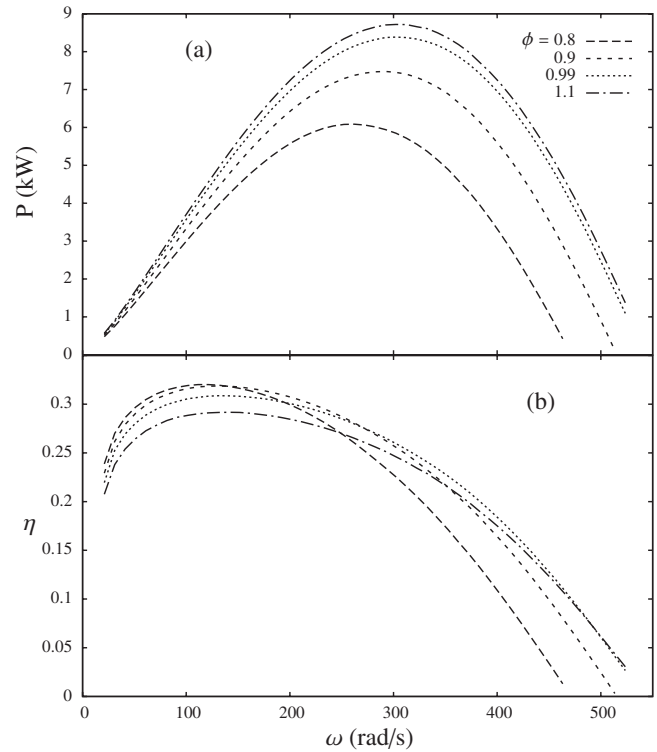

FIG. 4. Power output (a) and efficiency (b) of the simulated engine for several equivalence ratios ϕ ranging from lean to rich mixtures. Spark advance was considered at its ω-dependent optimal form $\bar{\varphi}_0(\omega)$, and cylinder internal wall temperature is constant, T_w=500 K.

B. Fuel ratio

The *fuel/air equivalence ratio* ϕ is defined as the ratio of the actual fuel/air ratio to the stoichiometric one. Apart from affecting power output and engine efficiency it has direct effects on pollutant emissions and spontaneous autoignition. It should be close to unity for satisfactory spark ignition and flame propagation. Lean fuel/air mixtures (ϕ less than unity) will burn more slowly and reach lower maximum temperature and also lower peak pressures. We shall explicitly see how engine performance, at any rotational speed, changes with ϕ. Moreover it is possible to get a relationship between fuel ratio and speed to optimize performance.

In Figs. 4(a) and 4(b) we plot a set of curves for power and efficiency, $P(\omega, \phi)$ and $\eta(\omega, \phi)$, respectively, obtained from our simulations for different values of fuel-air equivalence ratio ϕ. At any rotational speed power output increases as ϕ increases, but this is not true for the efficiency, which offers a more complicated behavior. At low ω (approximately up to 250 rad/s) more efficiency is obtained from low ϕ values, but for high ω this behavior is reversed. This fact can be explained by the presence of additional unburned fuel in the cylinder after combustion for high fuel ratios and low rotational speeds, so more fuel is needed to get the same power and then efficiency is lower [see Eq. (16)].

Figure 5 shows the plots $P(\eta, \phi)$ obtained by eliminating the rotational speed between $P(\omega, \phi)$ and $\eta(\omega, \phi)$. As we did in Fig. 2(c) for the spark advance angle, this figure allows a further optimization process although with some subtle differences, because the curves $P(\omega, \phi)$ do not present
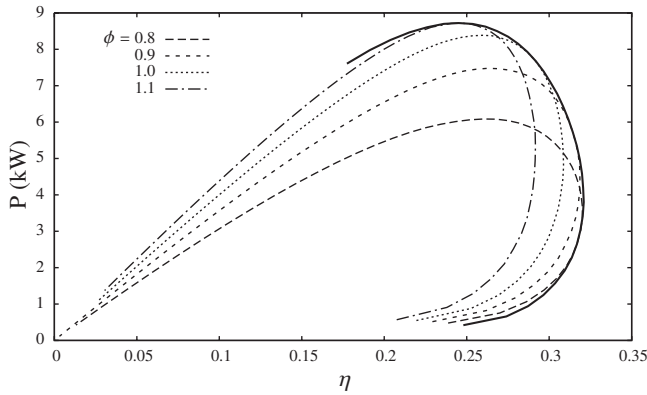
FIG. 5. Power-efficiency plots for several equivalence ratios with the same conditions as those in Fig. 4. The solid line represents the curve obtained with the optimal ω-dependent fuel ratio $\bar{\phi}(\omega)$, i.e., the fuel ratio giving for each required power output the maximum reachable engine efficiency.

an external envelope. Thus, now we look for the value of ϕ (and the corresponding ω), which, at a fixed power, gives the best compatible engine efficiency, i.e., we consider power as an externally fixed condition. For each value of power we look in Fig. 5 for the corresponding couple (ω_i, ϕ_i) giving the maximum efficiency. Mathematically this leads to a set of points (ω_i, ϕ_i), which can be interpolated to give an optimal function for fuel ratio, $\bar{\phi}(\omega)$. Once again we get a very simple linear form $\bar{\phi}(\omega) = 0.64 + 1.53 \times 10^{-3}\omega$ with ω in rad/s. Running the simulation with this velocity dependent shape for fuel ratio we obtain the shown envelope. As an illustrative example, for a power requirement of 7.5 kW, the curve $\phi = 0.9$ returns an efficiency $\eta = 0.26$, while from the external envelope (that for that power lies on the curve $\phi = 1.0$ approximately) we get an efficiency of 0.29, which represents an increase around 11%.

Moreover, it is interesting to study how changes in the fuel ratio affect losses associated with different irreversibility sources. In Fig. 6 we show $|W_{\text{fric}}|$, $|W_Q|$, and $|W_{\text{int}}|$. The addition of all work losses is represented as $|W_\ell|$. From this figure we stress three main points.

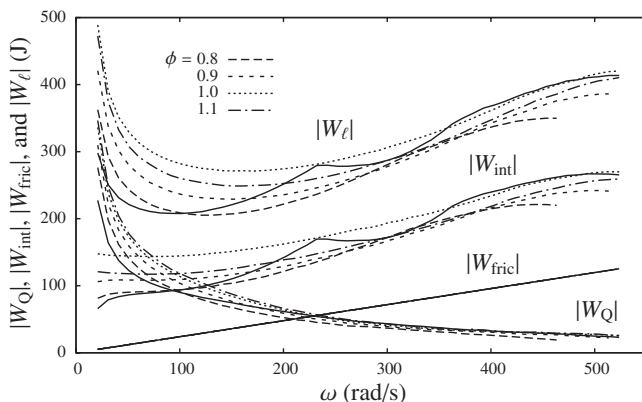(1) As happened for spark timing, at low engine speed, overall losses $|W_\ell|$ are dominated by $|W_Q|$, but when ω

FIG. 6. Analysis of work losses as function of engine speed for some fuel ratio values obtained with $\bar{\varphi}_0(\omega)$ and $T_w = 500$ K. For each type of losses, those obtained with the optimized ω-dependent fuel ratio $\bar{\phi}(\omega)$ are shown in solid line.

increases these losses quickly diminish. Simultaneously, $|W_{\text{fric}}|$ and $|W_{\text{int}}|$ increase, so $|W_\ell|$ shows a minimum around $\omega \simeq 100-200$ rad/s depending on the particular value of ϕ.

(2) Heat transfer losses increase with ϕ but the internal ones shows a subtle evolution with ϕ. They increase in the sequence $\phi = 0.8, 0.9, 1.0$. After the last one there is a change in behavior and for $\phi = 1.1$, $|W_{\text{int}}|$ is lower (and also $|W_\ell|$). This transition arises because $|W_{\text{int}}| = |W_{\text{rev}}| - |W_I|$ is strongly influenced by the adiabatic flame temperature T_3, which presents a maximum at stoichiometric fuel ratio, thus decreasing over stoichiometric conditions.

(3) At difference with spark advance, the optimization of fuel ratio $\bar{\phi}(\omega)$ does not yield to an envelope minimizing losses as a function of ϕ (see solid lines in Fig. 6) except at low values of ω. As noted before this is because the consideration of $\bar{\phi}(\omega)$ only accounts for the optimization of the efficiency at any fixed power. Then, the associated losses do not require to be minima.

C. Wall temperature

Engine heat transfer greatly affects engine performance and emissions. For a given rotational speed and a given mass of fuel inside the cylinder, an elevated heat transfer from the gas mixture to the cylinder walls decreases the average combustion, temperature, and pressure, and so the work per cycle transferred to the piston. In-cylinder heat transfer occurs by convection and radiation, but for spark ignition engines usually radiation is considered as negligible or subsumed into a convective heat transfer correlation.[29] In any case, heat transfer, as assumed in Sec. II B, is proportional to the temperature difference $T - T_w$, where T is the instantaneous temperature of the working fluid and T_w is the inner cylinder wall that usually is kept constant by the engine cooling system, but also depends on a complex form of combustion, which determines pressure and temperature inside the cylinder. Heat transfer occurs during the whole evolution of the engine (and so, we consider it in our simulations), but it is more relevant during combustion because temperature differences are greater.

We have performed an analysis of the influence of cylinder internal wall temperature T_w on the performance records of the engine, in the range between 400 and 700 K. We took the previously optimal values of spark advance $\bar{\varphi}_0(\omega)$ and fuel ratio $\bar{\phi}(\omega)$ for the simulations. Figure 7 shows a slight but interesting dependence of power output and efficiency on T_w. At low angular velocities, both functions take higher values for low temperatures: in the case of efficiency up to 240 rad/s and for power up to 310 rad/s. So, approximately for $\omega < 240$ rad/s, both higher power and efficiency are obtained with low T_w, and for $\omega > 310$ rad/s it is clear that higher performance parameters are obtained with high T_w.

But from these curves, it is not clear what happens in the interval between 240 and 310 rad/s, which is inside the region between maximum efficiency and maximum power
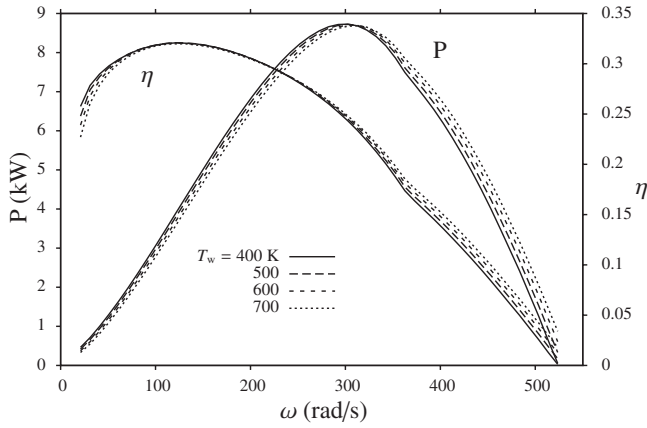
FIG. 7. Power, $P=P(\omega)$, and efficiency, $\eta=\eta(\omega)$, curves of the simulated engine for several cylinder internal wall temperatures, T_w (K). Spark advance and fuel ratio were considered at their ω-dependent optimal forms $\bar{\varphi}_0(\omega)$ and $\bar{\phi}(\omega)$, respectively.

points. This is probably the most adequate region for the stationary operation of any heat engine as argued by Chen.[30] But if we plot $P=P(\eta)$ by eliminating speed (Fig. 8), which appears in this region, it is always slightly better to keep a low internal wall temperature to get the maximum reachable efficiency for a particular fixed value of P. Then, this would be the optimal value for this parameter.

It is illustrative to look at the evolution of work losses with T_w. This is depicted in Fig. 9 as a function again of rotational speed ω. Friction losses in our model do not depend on temperature because as commented in Sec. II C we consider an effective temperature independent friction coefficient μ. Losses associated with internal irreversibilities neither depend on wall temperature, so the only influence of T_w, evidently, is observed in losses associated with heat transfer $|W_Q|$. It would be expected that work heat losses increase with the decreasing of T_w, because heat transfer linearly depends on the temperature gradient $T-T_w$. The figure shows the opposite evolution at low and intermediate values for ω (up to the point where there appears a crossing among curves, ~310 rad/s). We have checked that this effect is associated with combustion details. Particularly, because of two linked effects: During intake low wall temperatures re-
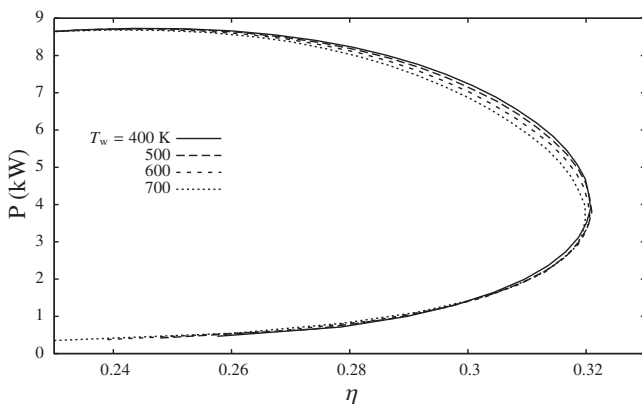

FIG. 8. $P=P(\eta)$ curves for several cylinder internal wall temperatures, T_w. Note that in the region between maximum efficiency and maximum power the lowest temperature, $T_w=400$ K, gives the best results: For a given power output it leads to the maximum achievable efficiency.
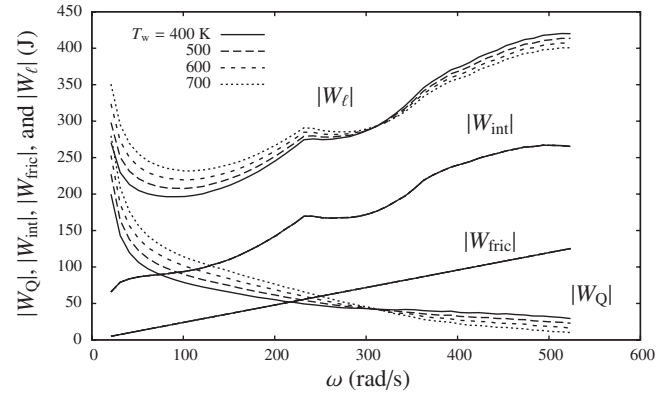

FIG. 9. Analysis of work losses as function of engine speed for some values of T_w obtained with ω-dependent optimal spark advance and fuel ratio $\bar{\varphi}_0(\omega)$ and $\bar{\phi}(\omega)$, respectively.

duces the heat transfer, therefore increasing the mixture density and more mass is charged per cycle. Also, the mass flux increases and consequently turbulent intensity grows up accelerating combustion process. So, for speeds below 310 rad/s (approximately the point where engine power output is maximum), heat transfer work losses are minimal for the lowest T_w while over that speed the behavior of heat transfer losses is opposite.

V. DISCUSSION AND CONCLUSIONS

By performing quasidimensional computer simulations and a finite-time thermodynamic analysis we have consecutively studied the effect of spark advance, fuel ratio, and cylinder internal wall temperature on the power output and on the efficiency of a spark ignition engine.

First, we have analyzed the influence of different spark advance angles and concluded that at any rotational speed it is possible to get a suitable speed dependent spark angle function $\bar{\varphi}_0(\omega)$ giving the maximum compatible values of efficiency and power, as represented by the external envelope in Fig. 2. Second, we have performed a study of the influence of the fuel ratio ϕ over the already spark advance optimized engine. By analyzing power-efficiency curves it is also feasible to build up a speed dependent optimum fuel ratio $\bar{\phi}(\omega)$, giving the maximum reachable efficiency for a certain power requirement (external envelope in Fig. 5). Third, we have finally analyzed the influence of the cylinder internal wall temperature T_w. Although neither maximum power output nor efficiency are very sensitive to T_w, it is interesting to stress that globally the temperature giving the most favorable $P=P(\eta)$ is the lowest one because it leads to better performance values in the region between maximum efficiency and maximum power values (see Fig. 8).

For each optimization step we have also investigated the influence of work losses associated with heat transfer through cylinder walls, frictions, and internal irreversibilities. Using macroscopic definitions coming from FTT we numerically calculated them from the simulations. As a summary for all the optimization steps it is clear how optimization is always related with the balance of heat transfer and internal irreversibility losses in the different rotational speed
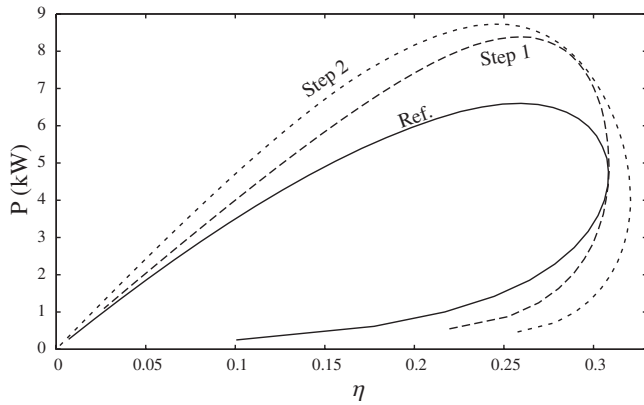
FIG. 10. $P = P(\eta)$ curves of the simulated engine obtained in the following way. Ref.: reference constant values of spark advance $\varphi_0 = 330°$, fuel ratio $\phi = 1.0$, and $T_w = 500$ K. Step 1: optimized ω-dependent spark advance $\bar{\varphi}_0(\omega)$, constant $\phi = 1.0$, and $T_w = 500$ K. Step 2: fully optimized values with ω-dependent spark advance $\bar{\varphi}_0(\omega)$, fuel ratio $\bar{\phi}(\omega)$, and optimum wall temperature $T_w = 400$ K. Note that in this last step the change in wall temperature T_w from the reference value does only introduce a small improvement in the region between maximum efficiency and maximum power conditions.

TABLE II. Values of maximum power, P_{max}, and maximum efficiency, η_{max}, in the three steps of the optimization procedure and values of the corresponding operating speeds, $\omega_{P_{max}}$ and $\omega_{\eta_{max}}$. Ref.: reference constant values of spark advance $\varphi_0 = 330°$, fuel ratio $\phi = 1.0$, and $T_w = 500$ K. Step 1: optimal ω-dependent spark advance $\bar{\varphi}_0(\omega)$, constant $\phi = 1.0$, and $T_w = 500$ K. Step 2: fully optimized values with ω-dependent spark advance $\bar{\varphi}_0(\omega)$, fuel ratio $\bar{\phi}(\omega)$, and wall temperature $T_w = 400$ K.

	$\omega_{P_{max}}$ (rad/s)	P_{max} (kW)	$\omega_{\eta_{max}}$ (rad/s)	η_{max}
Ref.	220.0	6.60	131.5	0.31
Step 1	302.4	8.39	131.5	0.31
Step 2	302.4	8.73	121.5	0.32

intervals. At low rotational speeds main losses arise from heat transfer, but they rapidly decrease and thus friction losses and mainly internal losses become the main source of irreversibilities at intermediate and high speeds.

It is quite illustrative to follow the different steps of our optimization in the usual framework of FTT. We assume power $P(\omega; \varphi_0, \phi, T_w)$ and efficiency $\eta(\omega; \varphi_0, \phi, T_w)$ as objective functions in terms of the rotational speed (the independent variable) and taking the spark angle, the fuel ratio, and the cylinder external wall temperature (φ_0, ϕ, and T_w, respectively) as control parameters. For some reference standard values of φ_0, ϕ, and T_w, and by means of a parametric elimination of ω we obtain a reference loop-shaped $P(\eta; \varphi_0, \phi, T_w)$ curve (see the solid line in Fig. 10). In our first optimization step we consider spark advance as a function of engine speed and obtain its optimum form $\bar{\varphi}_0(\omega)$, yielding to an improved power-efficiency curve $P(\eta; \bar{\varphi}_0(\omega), \phi, T_w)$ (see curve labeled step 1 in Fig. 10) in order to get more efficiency at any given power. In the second step we build up an optimum form for the fuel ratio considered as a function of ω, $\bar{\phi}(\omega)$, and so we get $P(\eta; \bar{\varphi}_0(\omega), \bar{\phi}(\omega), T_w)$. The dependence of these curves on cylinder internal wall temperature T_w is scarce. The most external curve of Fig. 10 considers the lowest temperature. This curve represents the fully optimized one.

In order to have a quantitative approach of the improvements on power and efficiency with our procedure we show in Table II the maximum power and maximum efficiency points of the curves contained in Fig. 10. Maximum power value after the first optimization step increases around 27% with respect to the reference simulation. In the fully optimized curve maximum power output is increased to 31% and maximum efficiency to 3% over the corresponding points in the reference curve.

In summary, in this work we have made use of the capabilities of both numerical simulations and theoretical tools from finite-time thermodynamics to optimize the performance of a spark ignition engine by analyzing the influence of some key parameters (spark advance angle, fuel ratio, and cylinder internal wall temperature) in the operation of the engine. The election of suitable spark angle and fuel ratio according to any fixed external power requirement could be valuable in order to get better spark ignition engines. We believe that this kind of studies where theoretical techniques and numerical simulations merge their analysis can be useful in the investigation and optimization of real spark ignition engines, not only with respect to engine operation but also for the design of the engine itself.

ACKNOWLEDGMENTS

[1] J. B. Heywood, *Internal Combustion Engine Fundamentals* (McGraw-Hill, New York, 1988).

[2] A. Bejan and E. Mamut, *Thermodynamic Optimization of Complex Energy Systems*, NATO Science Series (Kluwer, Dordrecht, 1999).

[3] R. S. Berry, V. Kazakov, S. Sieniutycz, Z. Szwast, and A. M. Tsirlin, *Thermodynamic Optimization of Finite-Time Processes* (Wiley, New York, 2000).

[4] L. Chen and F. Sun, *Advances in Finite-Time Thermodynamics* (Nova Science, Hauppauge, NY, 2004).

[5] S. Sieniutycz and P. Salamon, *Finite-Time Thermodynamics and Thermoeconomics* (Taylor & Francis, London, 1990).

[6] P. L. Curto-Risso, A. Medina, and A. Calvo Hernández, J. Appl. Phys. **104**, 094911 (2008).

[7] A. Fischer and K. H. Hoffmann, J. Non-Equilib. Thermodyn. **29**, 9 (2004).

[8] R. Stone, *Introduction to Internal Combustion Engines* (Macmillan, London, 1999).

[9] C. R. Ferguson, *Internal Combustion Engines, Applied Thermosciences* (Wiley, New York, 1986).

[10] C. Borgnakke, P. Puzinauskas, and Y. Xiao, Department of Mechanical Engineering and Applied Mechanics, University of Michigan, Technical Report No. UM-MEAM-86-35, 1986.

[11] D. Descieux and M. Feidt, Appl. Therm. Eng. **27**, 1457 (2007).

[12] J. M. Gordon and M. Huelihil, J. Appl. Phys. **72**, 829 (1992).

[13] L. Guzzella and C. H. Onder, *Introduction to Modeling and Control of Internal Combustion Engine Systems* (Springer, Berlin, 2004).

[14] H. Bayraktar and O. Durgun, Energy Sources **25**, 439 (2003).

[15] J. B. Heywood, *Internal Combustion Engine Fundamentals* (McGraw-Hill, New York, 1988), Chap. 3, pp. 80–81.

[16] J. C. Keck, in *Proceedings of the 19th Symposium (International) on Combustion* (The Combustion Institute, Pittsburgh, PA, 1982), pp. 1451–1466.

[17] N. C. Blizard and J. C. Keck, SAE Paper No. 740191, 1974.

[18] G. P. Beretta, M. Rashidi, and J. C. Keck, Combust. Flame **52**, 217 (1983).

[19] J. B. Heywood, *Internal Combustion Engine Fundamentals* (McGraw-

Hill, New York, 1988), Chap. 14, pp. 771–773.

[20]G. Eichelberg, Engineering (London) **148**, 463 (1939).

[21]A. Calvo Hernández, A. Medina, J. M. M. Roco, and S. Velasco, Eur. J. Phys. **16**, 73 (1995).

[22]F. Angulo-Brown, J. A. Rocha-Martínez, and T. D. Navarrete-González, J. Phys. D **29**, 80 (1996).

[23]F. Angulo-Brown, T. D. Navarrete-González, and J. A. Rocha-Martínez, in *Recent Advances in Finite-Time Thermodynamics*, edited by C. Wu, L. Chen, and J. Chen (Nova Science, Commack, NY, 1999).

[24]R. Stone, *Introduction to Internal Combustion Engines* (Macmillan, London, 1999), Chap. 3, pp. 62–68.

[25]J. B. Heywood, *Internal Combustion Engine Fundamentals* (McGraw-Hill, New York, 1988), Chap. 2, pp. 51–53.

[26]J. R. Senft, *Mechanical Efficiency of Heat Engines* (Cambridge University Press, Cambridge, 2007).

[27]B. J. McBride and G. Sanford, Users Manual 1311, National Aeronautics and Space Administration, NASA, http://www.grc.nasa.gov/WWW/CEAWeb/, 1996.

[28]J. B. Heywood, *Internal Combustion Engine Fundamentals* (McGraw-Hill, New York, 1988), Chap. 15, pp. 827–829.

[29]R. Stone, *Introduction to Internal Combustion Engines* (Macmillan, London, 1999), Chap. 10, pp. 429–433.

[30]J. Chen, J. Phys. D **27**, 1144 (1994).